Available online at www.sciencedirect.com

ScienceDirect

IFAC Papers Online CONFERENCE PAPER ARCHIVE

IFAC PapersOnLine 54-1 (2021) 1230–1235

Real-time velocity regulation for productivity optimization in laser cutting

Matteo Pacher [*,***] **Silvia Strada** [**] **Mara Tanelli** [**]
Barbara Previtali [***] **Sergio M. Savaresi** [**]

[*] *Adige S.P.A., BLMGROUP, Via per Barco 11, 38056, Levico Terme (TN), Italy*
[**] *Politecnico di Milano, Dipartimento di Elettronica, Informazione e Bioingegneria, Pizza Leonardo da Vinci, 32, 20133 Milano, Italy*
[***] *Politecnico di Milano, Dipartimento di Meccanica, Via La Masa 1, 20156 Milano, Italy*

Abstract: Laser cutting is an advanced industrial process, which has become the leading manufacturing technology for metal sheet processing, as it offers high flexibility and good productivity levels compared with other competing technologies. When the metal cutting process is performed in open-loop, though, to ensure that the desired quality levels are met, the cut is generally not performed at the maximum possible cutting speed and consequently its throughput is not the highest. To optimize productivity, two steps must be undertaken: first of all a reliable estimate of current cutting quality must be available online and, secondly, a closed-loop controller should regulate the cutting speed so that the desired quality is achieved. This work presents the design and the experimental validation of the full estimation and control architecture needed to regulate the cutting quality in terms of dross attachment, which is the main defect in this type of manufacturing process.

1. INTRODUCTION

In the context of metal sheet and thin tubes cutting, as in car-body making, shearing, blanking and stamping, the laser cutting technology has become the leading one, if compared with existing alternatives such as abrasive water jet cutting and electrical discharge machining, mainly due to its higher flexibility and enhanced productivity levels. In the cutting of metals, two main modes exist, which differ in the employed assisting gas. In particular, *oxidation* cutting occurs when oxygen is used, while *fusion* cutting in the case of nitrogen, Caristan [2004], Steen and Mazumder [2010], Pocorni et al. [2017]. Both these cutting modes are extensively used in the industrial panorama, even though in the last years fusion cutting is outpacing the oxidation one thanks to the increasing laser power availability. This work focuses on the design of an active control system that can optimize the productivity levels of the fusion cutting mode. Optimizing productivity means finding the optimal trade-off between quality and production speed, and realize a system that automatically regulates the process to operate at such an optimal point. In laser cutting, quality is traditionally determined considering different quantities, namely, dross attachment, kerf width, surface roughness, heat affected zone and presence of burns on the cut edge, Caristan [2004]. However, these aspects are not equally important: in particular, several works demonstrated that dross attachment is the most influential output in determining the overall process quality, see Pacher et al. [2017], Goppold et al. [2016]. Thus, in this work, dross attachment is selected as process output, and an innovative estimation procedure is proposed to obtain a real-time estimate of such quantity from data acquired from a high definition camera installed on the laser head. Advanced image-processing combined with machine learning allow to obtain a continuous variable that represents the output of interest. Further, a speed-regulation controller is designed to track a desired dross attachment level, and closed-loop experiments are carried out to test the validity of the approach. This closed-loop system has several advantages over current practice. In fact, nowadays, process parameters are experimentally optimized to obtain high-productivity and high-quality cuts. However, this open-loop tuning method has some intrinsic limitations. Cutting speed is normally decreased with respect to the maximum allowable to improve robustness, thus yielding suboptimal productivity levels. Furthermore, quality degradation may be experienced due to either aging of the optical components or to a significant difference in the processing conditions between the optimization phase and the real practice. Thus, to obtain results that are repeatable over the machine life and across the different working conditions, a feedback control approach such as that presented herein is key. Despite other contributions in the field such as Duflou et al. [2009], Sichani et al. [2010], note that the proposed solution is the first example of closed-loop control for the *continuous* regulation of process quality in this field. The most significant feature of the proposed approach lies in the capability of the final system not only to avoid dross formation, but it can be used to regulate dross to a desired level. This opens the possibility of customizing the process behavior and of letting the user govern the trade-off between quality and productivity.

The structure of the paper is as follows. Section 2 describes the experimental setup considered in this work and defines the considered control problem. Section 3 discusses how the dross attachment estimation is performed. Then, Section 4 presents the identification of the process dynamics, and Section 5 illustrates the controller design and the related experiments.

2. PROBLEM STATEMENT AND DESCRIPTION OF THE DROSS ATTACHMENT MONITORING ARCHITECTURE

An industrial laser cutting machine has been used in the experiments. It is endowed with a fiber laser source that can deliver up to 6 kW of power and has a fiber core diameter of $d_{core} = 100\,\mu$m. The machine mounts

10.1016/j.ifacol.2021.08.146

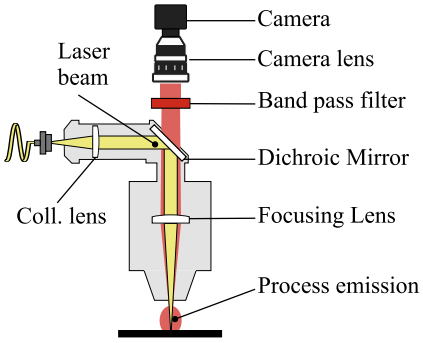

Fig. 1. Scheme of the monitoring architecture installed on the laser cutting head.

a standard cutting head that has been customized for monitoring purposes (see Fig. 1).

The monitoring architecture is composed of a camera, with appropriate filters and mounted coaxial to the laser beam. The selected camera sensor is an industrial CMOS camera; sensor size and pixel size are 1280 px × 1024 px and 4.8 µm × 4.8 µm, respectively. The camera lens and the number of pixels were selected to have a field of view of 2 mm × 2 mm and a spatial resolution of 9.6 µm/px. Considering the performance of the camera, monochrome images of size 210 px × 210 px were acquired at 1500 fps; further, based on the existing scientific literature, Duflou et al. [2009], Mazzoleni et al. [2019], Pacher et al. [2019], a near infrared wavelength range was selected. A microcontroller was used to acquire the process parameters (*e.g.*, cutting speed, laser power, etc.) at a sample rate of 10 kHz and for producing a TTL signal to be used as trigger for the image acquisition; this eventually permits to perfectly synchronize images and process inputs. To measure the dross attachment a microscope having resolution equal to 5 µm and field of view of 23 mm × 17 mm has been used.

To study and monitor the dross attachment formation, different experiments have been carried out where the goal was to produce a *large* quality variation in order to collect both dross-free (good-quality) and high-dross (low-quality) cuts. During the experiments, a standard squared specimen with side length of 45 mm was selected and two materials, namely, stainless steel X5CrNi18-10 and mild steel S235JR were cut for thicknesses ranging from 3 to 10 mm. The laser power was kept constant at 6 kW whereas cutting speed, gas pressure and focal position were varied to obtain different levels of dross attachment.

3. REAL-TIME DROSS ESTIMATION

This section illustrates how a real-time dross estimate is made available to the control system, outlining all the key steps.

3.1 Definition of the dross measure

A quantitative measure of dross attachment is fundamental for the design of an online estimation algorithm, as it allows both to train and to validate/test the model. In fact, when developing the estimator, there is the need to quantitatively map features obtained from the monitoring chain to a variable representing the true amount of dross produced. Hence, the objective dross measurement is needed whenever a new material or a new sheet thickness appears. To construct the mentioned map, the whole specimen's profile is considered. Due to the reduced field of view of the microscope, three pictures with partial overlapping of each side are collected and then stitched together.

According to the measurement procedure, the thickness profile $T(d)$ in Fig. 2 is expressed as a function of the horizontal abscissa d in the spatial domain. Let us consider a discrete-time abscissa $k = i\Delta t,\ i \in \mathbb{N}$ where k is the discrete time abscissa and Δt is the sampling period. The displacement as a function of time, $d(k)$, is computed by integrating the feed rate so that the thickness profile can be expressed in the time domain, as

$$T(d) = T(d(k)) = T(k)\,. \tag{1}$$

The thickness T is made of both the nominal thickness of the sheet, T_n, and the dross attachment. As the nominal thickness is known, the dross attachment profile, $h(k)$, can be computed as

$$h(k) = T(k) - T_n\,. \tag{2}$$

Finally, to emphasize the dross droplets with respect to the thickness baseline, the dross profile has been squared, yielding

$$h^2(k) = \left(T(k) - T_n\right)^2\,. \tag{3}$$

So, starting from the dross measure, a dimensionless quantity for online estimation is defined, which may eventually become the system output employed for future control purposes. This quantity has the advantage to describe the dross attachment in a more general way with respect to the traditional measurement of the dross height.

To set the significant dross height according to the judgment of skilled technicians, 100 specimens of different materials and with different thickness were analyzed. For each specimen, a binary indicator of dross (dross presence or not) was obtained, and, considering these judgments, a threshold value, h_0^2, for the quantity $h^2(k)$ was determined. In Fig. 3, two examples of dross-free and mid-dross cuts are shown together with the resulting threshold value. Once the threshold value has been set, the quantity $h^2(k)$ can be transformed to a binary signal indicating the appearance of significant droplets, *i.e.*,

$$h_{th}^2(k) = \begin{cases} 1 & h^2(k) > h_0^2,\ k \geq 0 \\ 0 & \text{otherwise} \end{cases}\,, \tag{4}$$

where $h_0^2 = 0.03\,\text{mm}^2$. The quantity $h_{th}^2(k)$ is dimensionless and can be useful to train and test classification algorithms. However, it takes just binary values and it will not permit a continuous regulation of the dross amount to a desired value. Therefore, the system output is defined as the moving average of $h_{th}^2(k)$

$$y(k) = \frac{1}{\gamma+1}\sum_{j=0}^{\gamma} h_{th}^2(k-j)\,, \tag{5}$$

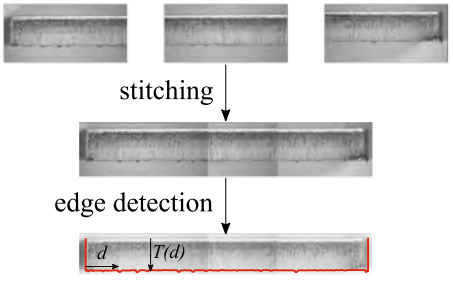

Fig. 2. Image elaboration steps for dross attachment measurement. d is the horizontal coordinate for each side and T is the thickness including dross attachment.

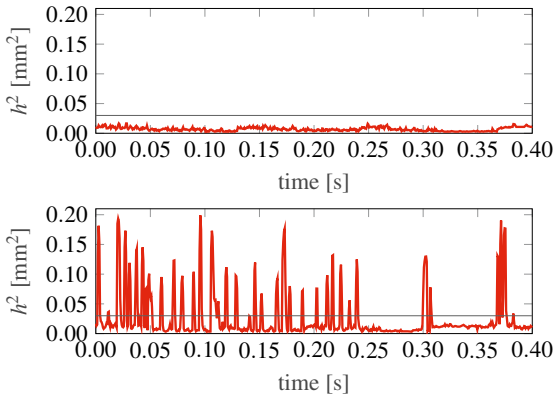

Fig. 3. Comparison between a dross-free and a mid-dross cut. The threshold value is also shown.

where γ is the size of the look-back window. The signal $y(k)$ is continuous and bounded within the interval [0, 1]. In further research also different, more sophisticated filtering operations could be considered. It indicates how frequent is the appearance of significant dross droplets (*i.e.*, above the threshold h_0^2) within a time interval of $\gamma\Delta t$. As a result, this quantity puts together the dynamic behavior of dross attachment with its significance in terms of magnitude. This signal, $y(k)$, constitutes the final quantitative measure of dross attachment that has to be estimated in real time.

3.2 Indirect estimation of the dross profile via image analysis

The continuous and dimensionless quantity $y(k)$, previously identified as the quantitative measure of dross attachment, has to be estimated online, $\hat{y}(k)$, relying on the process emission captured by the coaxial camera, in order to be employed for further feedback control purposes. The estimation procedure illustrated in this section consists of the series of two main processing phases: *featuring* and *mapping*. *Featuring* consists of deriving a compact geometrical description (features) from the raw images of process emission, while *mapping* means the processing of such limited number of features onto the dross attachment estimate, $\hat{y}(k)$, which is the pursued final output of the overall estimation stage.

Featuring Phase Estimation starts with the extraction of a limited number of geometrical quantities and of the luminosity from the images captured by the camera focusing on the laser irradiated zone during the cutting process.
Each image, represented at first by a matrix of grey levels, is binarized according to a static threshold, chosen iteratively to emphasize the phenomena that are close to the melting temperature (which is almost the same) of the two studied materials. The resulting binary (black and white) image has the same size as the original one and is characterized by a set of white points, called *blob*, a kind of footprint with two differently long tails, representing the laser irradiated zone of the metal specimen.
After the original image intensity, I, is calculated adding up by rows and by columns each point grey level, three other blob related, explicative geometrical quantities are calculated with an ad hoc designed algorithm:

(1) blob centroid, c, that is the center of mass of the blob;
(2) blob width, w, that is the maximum dimension of the blob perpendicular to the cutting direction;

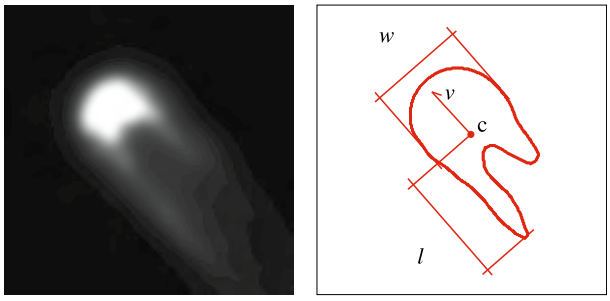

(a) Process emission image. (b) Extracted geometrical features.

Fig. 4. Application of the image analysis algorithm for the extraction of geometrical features and of binary intensity from the laser irradiated zone.

(3) blob length, l, that is the maximum dimension of the blob parallel to the cutting direction extending from the centroid to the blob longest tail endpoint.

These features were selected by observing some trend in the videos for different dross attachment conditions. High-dross cuts are usually characterized by an elongated blob shape and by a greater variation in its length. Conversely, dross-free cuts are characterized by a stable and usually smaller blob shape.
In Fig. 4, an example of the three main steps of the *featuring* phase are depicted. The computational time for processing one image with compiled code implemented in Matlab run on a Dell XPS with an Intel i7 processor is approximately 0.3 ms. As a result, real-time image featuring is feasible being the target image acquisition rate equal to 1500 fps corresponding to a sampling period of approximately 0.67 ms.
Applying the *featuring* processing to a complete cut yields the three time signals, $w(k)$, $l(k)$ and $I(k)$. Only the portions of the cut geometry having constant process parameters are considered. The transients due to the path corners are neglected as shown in Fig. 5 .

The intensity, blob width and blob length time varying features have to be now linked to the quasi-steady-state dross attachment formation in the corresponding quasi-steady-state locations.
To overcome the scarce appropriateness of looking for a relationship between each k-sample of the image descriptors and the dross attachment, the sample stochastic distribution, over a time interval τ, for each feature is

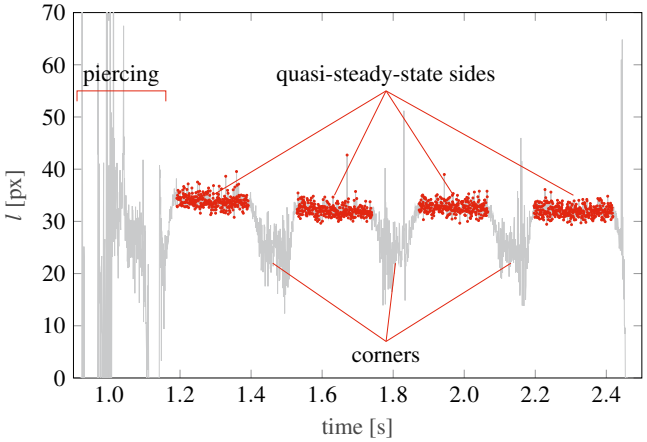

Fig. 5. Example of a width l time signal. The steady-state part only is considered for quality estimation.

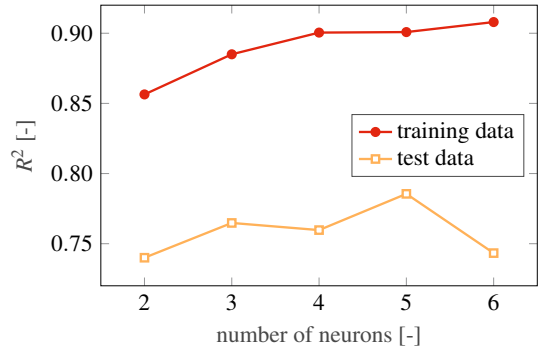

Fig. 6. Evaluation of the fitting peformance: value of R^2 as a function of the number of neurons.

considered. These distributions are not easily described by conventional parametric ones; as a consequence, they are more compactly represented by their mean value, their variance and their skewness. As a result, the image features employed for process output estimation are 9, that is 3 statistical indicators times the 3 features {w, l, I}. Since the estimation of the dross attachment has to be performed and updated in real time, a backward sliding time window, τ, is used to evaluate the 9 mentioned statistical features at each time instant k. As a consequence, the lower τ, the weaker are the low-pass filtering effects in the prediction dynamics and the prompter the activation of the connected control system.

Mapping Phase The purpose of the *mapping* phase is to model the dependency of the dross attachment estimate, $\hat{y}(k)$, from the 9 statistical features (from intensity, width and length sample distributions).
In this work, an Artificial Neural Network (ANN) is used as mapping tool, since ANNs do not require the formulation of a parametric model and their complexity can be controlled by limiting the number of neurons and layers of the net, also to avoid overfitting. Linear regression models have also been tested and compared to ANNs, in a preliminary design phase; they resulted to be less accurate and to provide worse extrapolation capabilities. During the *mapping* phase, under the assumption of a unique model structure for our contained set of materials/thicknesses, model parameters for each thickness, $3\,mm$ and $5\,mm$, have to be identified. It must be noted that the variability range of the regulated process velocity is sufficiently narrow so that, once the models' parameters have been estimated, the estimate is sufficiently precise across the whole operational interval without the need of adaptation. A simple ANN structure with a single hidden layer was selected and, starting from the 9 inputs to the NN, the number of hidden neurons and the sliding window τ where

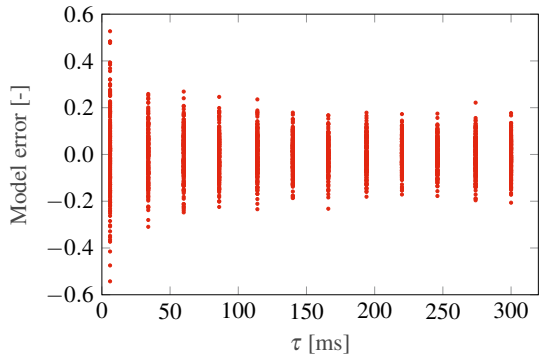

Fig. 7. Model error as a function of the window-length τ.

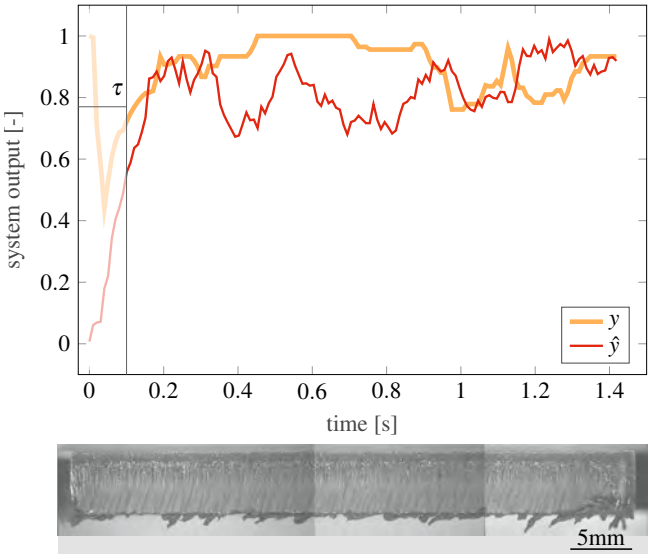

Fig. 8. Dross attachment estimation results in a $5\,mm$ stainless steel high-dross cut: time histories of the true dross $y(k)$ and of the estimated on $\hat{y}(k)$ and picture of the cut specimen.

selected iteratively, by performing sensitivity analysis. It was experimentally proven that the model accuracy stabilizes from 5 hidden neurons on and for a time window of approximately $100\,ms$, see Fig. 6 and Fig. 7, which were chosen as final values for both parameters.

Evaluating iteratively all the features' combinations, the triplet composed of the mean values of blob length, width and intensity was selected as the most informative one. Thanks to the high time resolution of the camera, the two models rely on approximately 25000 and 35000 data points for $3\,mm$ and $5\,mm$, respectively. These datasets were split in the three sets for network training, validation and testing with percentages 80%, 10% and 10%, respectively.

Estimation results The results of the ANN based dross attachment estimation algorithm is shown in Fig. 8, which shows both the estimate $\hat{y}(k)$ and the true dross attachment $y(k)$ for a $5\,mm$ stainless steel high-dross cut (cutting speed $v = 6\,m\,min^{-1}$). The cut specimen is also shown below for visual reference. Overall, the prediction model ensures good performance and the model error remains almost always below 0.1 even in this challenging case. Even better results are obtained for the 3mm case.

4. EXPERIMENTAL IDENTIFICATION OF THE PROCESS DYNAMICS

The identification of the cascade of process and estimator dynamics is a crucial step for controller design. As previously described, the control variable of the proposed control scheme is the cutting speed, v, while the controlled variable is the prediction of the dross production $\hat{y}$. Accordingly, the dynamics of interest can be expressed as a transfer function $G(s)$, linking the input v and the output $\hat{y}$. To estimate $G(s)$ a frequency-domain parametric identification approach is used. The bandwidth of the open-loop system depends on the bandwidth of the estimator and on the machine actuators. In principle, a control algorithm could potentially run at a really high sampling rate. In fact, after a time equal to the look-back window, *i.e.*, $\tau = 100\,\text{ms}$, the estimate of dross is available at the same sampling rate of the camera, hence at 1500 fps.

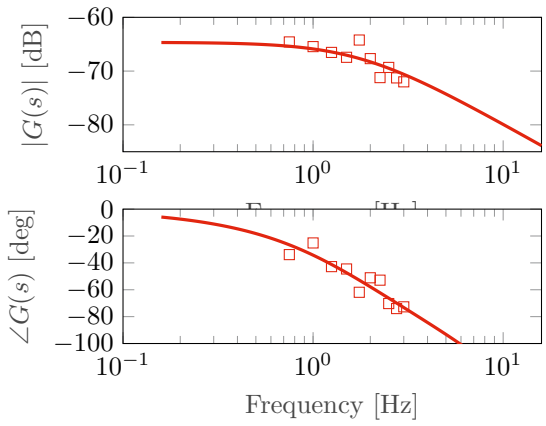

Fig. 9. Results of the system identification fitting procedure.

However, in the available HW setup, the connections between the controller and the machine are made via analog signals. Thus, the control input v must be appropriately computed and transformed into a voltage command to the machine. The numerical control of the machine runs in the order of hundreds of Hertz, but after experimental evidence, the bandwidth of the full actuation chain is estimated to be only of 7.5 Hz, probably due to limitations in the analog to digital conversion step. This poses severe limitations to the achievable closed-loop response time and to the frequency range for system identification. Due to this limitations, the desired bandwidth of the controlled system has been set to 1 Hz. Ongoing work is focused at enhancing the overall performance to reach a bandwidth of approximately 100 Hz, which is in principle achievable with an improved experimental setup.

Due to the frequency limitations of the specific system's actuators, the identification experiments are performed cutting along a simplified and longer geometrical path. The cut geometry consists of a straight line of length 400 mm on a stainless steel X5CrNi18-10 specimen with thickness 3 mm. Process parameters are set according to previous experiments and only the cutting speed is varied. The high-speed dross attachment window of the process is considered; in this region, dross attachment increases with the cutting speed before going towards plasma induced cut. The low-speed dross attachment is accordingly neglected because in practice the role of a feedback control system would be to maximize the speed meanwhile tolerating an *acceptable* amount of dross.

System identification is performed in the frequency range $0.75 \div 3$ Hz with steps of 0.25 Hz, so that in this range the aliasing effect is limited. The cutting speed is constat during the cuts and varied from 6.9 m min^{-1} to 9.7 m min^{-1}. This speed range proved to produce dross-free to high dross cuts in the considered experiments.

Using the points of the experimental frequency response derived from data (see Fig. 9), a first order dynamical system with delay proved accurate enough to describe the overall system, at least within a low/medium-frequency range. The system model is thus

$$G(s) = \frac{\mu_G}{1 + s\,T_G}\, e^{s\tau_G}\,, \tag{6}$$

where the parameters are μ_G, T_G and τ_G representing the static gain, the time constant and the pure delay, respectively.

Given the very fast process dynamics, the pole and the static delay in the model are allegedly due to the estimator dynamics, which introduces low-pass filtering effects. In fact, the pure cutting phase should induce a dynamic response in the order of hundreds of Hertz due to the high-rate at which the material is melted by the laser beam, so outside the range currently analyzed in the experiments, and anyway much beyond the needed closed-loop bandwidth. A more thorough analysis of the two distinct dynamics will be carried out when higher-frequency excitation tests will be possible.

5. CLOSED-LOOP LASER CUTTING QUALITY REGULATION

A simple proportional controller $R(s) = K_p$ is chosen to demonstrate the possibility of a feedback approach for controlling the dross attachment behavior. This choice is motivated by the frequency limitations and the given system dynamics.

The value of the proportional gain is initially estimated as $K_p = 1800$ to meet the requirement of 1 Hz of bandwidth of the loop transfer function

$$L(s) = R(S)\,G(s) = K_p \frac{\mu_G}{1 + s\,T_G}\, e^{s\tau_G}\,. \tag{7}$$

In cascade to the controller, a saturation block is introduced to avoid unfeasible speed settings and to avoid acting in the low-speed dross process window. Control experiments are carried out to validate the capabilities of the presented methodology. The cut geometry is the same as for the identification experiments, *i.e.*, a straight line of length 400 mm.

During the experiments different constant dross set points are commanded to the controller, to investigate the capabilities of the controller in following an arbitrary quality requirement. The initial conditions, namely, the initial cutting speed is set according to the set point: for a low value of the set point, the initial speed is set to make the cut begin with high dross attachment. Conversely, for mid-high set point values, the initial cutting speed is set to have a low dross cut. This choice was made to better appreciate the closed-loop response induced by the controller. Figures 10-12 show three examples of feedback controlled dross attachment. In Fig. 10 a low dross setpoint is used; in the first part of the cut, the controller decreases the speed to decrease the amount of dross; the commanded value is then reached and maintained approaching the end

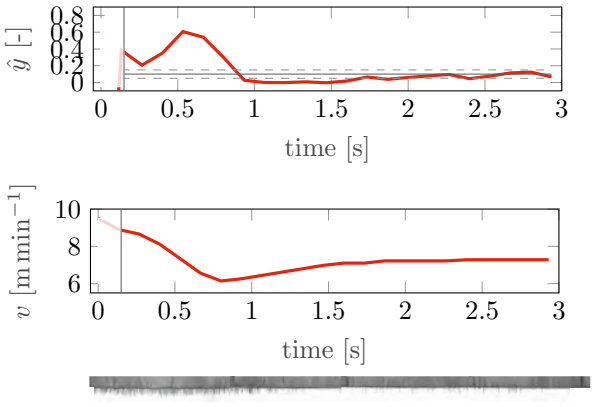

Fig. 10. Results of a controlled cut for a low amount of dross. The cut profile (not in scale) is shown together with input and output signals.

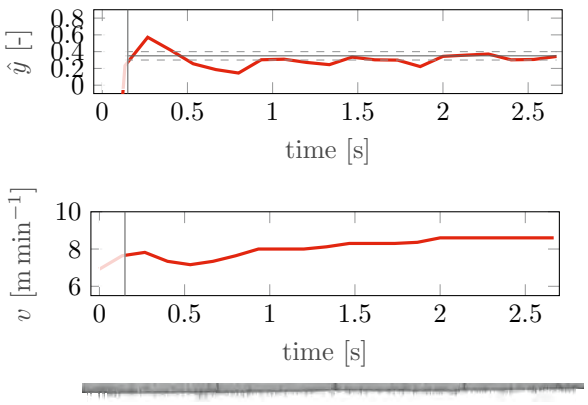

Fig. 11. Results of a controlled cut for an intermediate amount of dross. The cut profile (not in scale) is shown together with input and output signals.

of the cut by a slow increase of the cutting speed. In Fig. 11, an intermediate dross setpoint is set; in the first part of the cut, the speed is increased and then decreased making the estimate oscillate around the set point value. Then, cutting speed is slowly increased again so that the set point is reached and maintained untill the end of the cut.

Finally Fig. 12 shows the results obtained with a high value of the setpoint, that means a relatively major dross can be accepted; in the first part of the cut, the speed is significantly increased beacause of the quite high tolerated setpoint dross. Then, the cutting speed is more and more slowly raising to keep dross close to the set point for the rest of the cut.

Considering the experimental results in Fig.10-12, it is observed that the closed-loop system stabilizes at the setpoint value after approximately $t_s = 1.8$s. The system does not oscillate around the setpoint and the overshoot is $\leq 10\%$, meaning that the phase margin of the closed-loop system can be assumed to be ≥ 65deg. The cutoff frequency of the system can be estimated as $f_c \approx 0.5$Hz. These results are encouraging and demonstrate that the proposed approach is suitable to adjust the steady state value of the cutting speed according to the desired value of dross attachment. This allows to optimize productivity, by carefully selecting the dross level that is admissible in the given application, and to ensure that the maximum operational speed compatible with such a quality constraint is employed. Of course, the bandwidth of the closed-loop

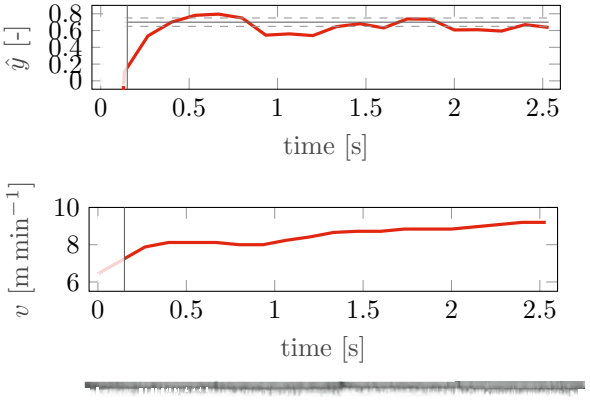

Fig. 12. Results of a controlled cut for a high amount of dross. The cut profile (not in scale) is shown together with input and output signals.

system has still to be increased to allow its full operational use in industrial machines.

6. CONCLUDING REMARKS AND OUTLOOK

This paper presented a full implementation of a control system for automatically adjusting the quality of laser cutting by controlling the speed at which the cut is performed. As quality parameter, the dross attachment is selected, and an advanced estimation of the controlled variable is presented, based on accurate processing of the images of a high-definition camera installed on the laser head. The overall system was tested with selected cut experiments, proving its applicability in an industrial context. Ongoing work is being devoted to enhance the existing HW setup in order to obtain higher sampling frequencies, which will enable a more extensive testing of the overall closed-loop system.

ACKNOWLEDGMENTS

The authors gratefully acknowledge BLMGROUP for the great cooperation and for their professional support. The presented study has been funded with the contribution of the Autonomous Province of Trento, Italy, through the Regional Law 6/99. Name of the granted Project: LT4.0.

REFERENCES

Caristan, C.L. (2004). *Laser Cutting Guide for Manufacturing*. Society of Manufacturing Engineers, Dearborn, Michigan.

Duflou, J.R., Sichani, E.F., Keuster, J.D., and Kruth, J.P. (2009). Development of a real time monitoring and adaptive control system for laser flame cutting. *International Congress on Applications of Lasers & Electro-Optics*, 2009(1), 527–536.

Goppold, C., Pinder, T., and Herwig, P. (2016). Transient beam oscillation with a highly dynamic scanner for laser beam fusion cutting. *Advanced Optical Technologies*, 5(1), 61–70.

Mazzoleni, L., Demir, A.G., Caprio, L., Pacher, M., and Previtali, B. (2019). Real-Time Observation of Melt Pool in Selective Laser Melting: Spatial, Temporal and Wavelength Resolution Criteria. *IEEE Transactions on Instrumentation and Measurement*, 1–1.

Pacher, M., Mazzoleni, L., Caprio, L., Demir, A.G., and Previtali, B. (2019). Estimation of melt pool size by complementary use of external illumination and process emission in coaxial monitoring of selective laser melting. *Journal of Laser Applications*, 31(2), 022305.

Pacher, M., Monguzzi, L., Bortolotti, L., Sbetti, M., and Previtali, B. (2017). Quantitative identification of laser cutting quality relying on visual information. In *LiM 2017 Proceedings*, 1–11. Munich.

Pocorni, J., Kaplan, A.F.H., Petring, D., and Powell, J. (2017). *LIA Guide to High Power Laser Cutting*. Laser Institute of America, Orlando, FL.

Sichani, E.F., De Keuster, J., Kruth, J.P., and Duflou, J.R. (2010). Monitoring and adaptive control of CO2 laser flame cutting. *Physics Procedia*, 5, 483–492.

Steen, W.M. and Mazumder, J. (2010). *Laser Material Processing*. Springer, London, 4th edition edition.